IEEE Access
Multidisciplinary ⋮ Rapid Review ⋮ Open Access Journal

Received December 8, 2020, accepted December 12, 2020, date of publication December 17, 2020,
date of current version December 31, 2020.

Digital Object Identifier 10.1109/ACCESS.2020.3045443

Clifford Geometric Algebra-Based Approach for 3D Modeling of Agricultural Images Acquired by UAVs

PRINCE WAQAS KHAN[1], YUNG-CHEOL BYUN[1], AND MUHAMMAD AHSAN LATIF[2]
[1]Department of Computer Engineering, Jeju National University, Jeju 63243, South Korea
[2]Department of Computer Science, University of Agriculture Faisalabad, Faisalabad 38000, Pakistan

Corresponding author: Yung-Cheol Byun (ycb@jejunu.ac.kr)

This work was supported by the Korea Institute for Advancement of Technology (KIAT) Grant funded by the Korean Government [Ministry of Trade, Industry and Energy (MOTIE)] (The Establishment Project of Industry—University Fusion District) under Grant N0002327.

ABSTRACT Three-dimensional image modeling is essential in many scientific disciplines, including computer vision and precision agriculture. So far, various methods of creating three-dimensional (3D) models have been considered. However, the processing of transformation matrices of each input image data is not controlled. Site-specific crop mapping is essential because it helps farmers determine yield, biodiversity, energy, crop coverage, etc. Clifford Geometric Algebraic understanding of signaling and image processing has become increasingly important in recent years. Geometric Algebraic treats multi-dimensional signals in a holistic way to maintain relationship between side sizes and prevent loss of information. This article has used agricultural images acquired by unmanned aerial vehicles (UAVs) to construct three-dimensional models using Clifford geometric algebra. The qualitative and quantitative performance evaluation results show that Clifford geometric algebra can generate a three-dimensional geometric statistical model directly from drones' RGB images. Through peak signal-to-noise ratio (PSNR), structural similarity index measure (SSIM), and visual comparison, the proposed algorithm's performance is compared with latest algorithms. Experimental results show that proposed algorithm is better than other leading 3D modeling algorithms.

INDEX TERMS Clifford algebra, computer vision, geometric algebra, image processing, precision agriculture, quaternions, remote sensing, 3D images, unmanned aerial vehicles.

I. INTRODUCTION

With the advent of information technologies such as computer vision image processing and precision agriculture, farmers can increase their productivity. Precision agriculture allows farmers to apply necessary processing methods more accurately by collecting various data from the land to understand temporal and spatial changes of production resources [1]. Remote sensing is beneficial tool for monitoring and assessing yield of various crops [2]. This includes real-time and rapid screening of crop varieties, food security [3], social and economic stability, jobs, and environmental services [4]. Remote sensing of crops using hyperspectral vision is first type of spectral imaging used to identify and classify crops [5]. With the advent of drones, breakthroughs have been made in land cover mapping and classification. Unmanned Aerial Vehicles (UAVs) can obtain very high spatial and temporal resolution images at relatively low cost than manned operated aerial systems or satellite systems [6]. However, it is not straightforward to reconstruct phenomena based on size and topological relations. The development of three dimensional (3D) and temporal Geographic Information Systems (GIS) helped to analyze high dimensional data, computational complexity, and increase scalability.

Clifford algebra, also known as geometric algebra (GA), was developed by William Kingdon Clifford [7]. Since its appearance, many researchers have used it to deal with time and space issues in physics. Clifford algebra has developed into more sophisticated geometric approach. Many researchers have applied Clifford's algebra approach to the field of information processing with computer technology advancement, including computer vision, robotics, and image processing, in which remarkable results were accomplished [8]. Sau *et al.* [9] applied Clifford algebra

The associate editor coordinating the review of this manuscript and approving it for publication was Yiming Tang.

and quaternion approach, a sub-algebra of Clifford algebra, to image compression by splitting image into three color planes. In work by Jayme *et al.* [10], they discuss Clifford algebra for 3D Euclidean space. They explained different operations such as transformations of points, reflection, shear transformation rotations, and translation from Clifford algebra's viewpoint. Liu *et al.* [11] proposed a method for indoor 3D reconstruction using smartphones using Clifford geometric algebra. Smartphone sensors are used to measure azimuth and pitch angles. Then through these angles, the space of indoors display can be adequately modeled. The independently reconstructed patterns are then joined together to form complete model. At the same time, isometric algebra is used as a computational structure. Compared with other reconstruction methods, the use of isometric geometric algebra simplifies geometry and combines various geometric relations. Yet the biggest obstacle in integrating GIS and geographic models is that the foundations of GIS and geographic models are geometry and algebra, respectively, making it difficult to integrate different types of geospatial data structures [12]. For example, vector data, spatiotemporal field data, and network data. To integrate such data types, there is no rigid mathematical background available [13]. GA is a natural tool to connect the two. Therefore, rewriting the existing geographic models under GA framework creates tighter integration of GIS and geographic modeling. We have integrated the existing reconstruction model with Clifford algebra to obtain real-world agricultural modeling system. This article has used agricultural images acquired by unmanned aerial vehicles to construct three-dimensional models using Clifford geometric algebra. The main contributions of this article are

- Introducing more simplified and unified data structures for Geo-computing based on GA;
- Building an expressive, complete, and accurate data model for real-world agricultural modeling;
- Providing a significant demonstration and application of UAVs in agriculture.

The remainder of the article is composed as follows: Section 2 introduces relevant publications and articles. Section 3 describes proposed Clifford geometric algebra-based 3D modeling approach, including data collection process. We have compared the presented approach results with the other approaches in section 4, and Section 5 concludes the article.

II. RELATED LITERATURE

UAV systems offer many benefits in various mapping applications, such as tilt mapping and geographic disaster investigation. Cahyono *et al.* [14] focused on rotor drones because the rotor unit is stable and easy to capture images. According to the aerial photography program, 60 photographs were taken with striped aerial photographs. Auxiliary data from ground control points using GPS geodetic surveys and checkpoints set using total station technology. Calibrate digital camera using short-range photogrammetry software and use restored camera calibration parameters for digital image processing. It uses digital photogrammetry software to process all aerial photographs and output them in orthogonal format. Combining the aerial survey function of unmanned aerial vehicles with unmanned ground vehicles' target intervention function can greatly improve automation systems' efficiency applied to precision farming. It is important to set up and update common domain map, but it is not easy in this case. Maps generated by different types of robots show differences in size, accuracy, and scale, and the relevant geographic location data may be inaccurate and biased. However, in an agricultural environment, it seems obvious. Both iterations of engineering structure defeated the classic map fusion technique. Potena *et al.* [15] solved the problem of cooperative UAV environment reconstruction and unmanned ground vehicle environment reconstruction in agricultural fields by proposing an effective method for aligning non-uniform three-dimensional maps. Their method represents multimedia environment using target domain semantics, geometry, and data linking strategies. They reported comprehensive tests proving that their method is superior to the standard method. Computer vision has been successfully used to destroy weeds between crops mechanically. Assuming known locations of crop rows and assumption that plants growing outside these locations are weeds can be used in this system. However, for many crops, automatic weeding of continuous or crop groups with mixture of weeds and plants is not resolved randomly. The purpose of Piron *et al.*'s study [16] was to measure that plant's height is the difference between early-growing crops and weeds because weeds and crops grow at different rates. Plant height uses active holographic technology based on multi-emitter code modulator illumination developed for small scene features. There were several kinds of hubs at the point of data collection. Considering ground's non-uniformity, a new parameter called ''corrected plant height'' is calculated to represent plant height accurately. This parameter is the distance between observed pixel and the actual ground level below it.

3D tree structures play an important role in many scientific fields, such as study of forests and agriculture. Laser ground view scanning can effectively display 3D spatial locations and tree structures in point clouds. Several methods have been proposed in literature to restore 3D trees in ground-based laser scanning point clouds. However, in general, it is not possible to review incomplete laser scanning data. To address such incomplete terrestrial laser scanning data sets, a new method based on structure-aware global optimization approach is proposed by Wang *et al.* [17] The proposed method first estimates tree skeleton in shortest time and uses tree skeleton to determine the extension direction. The proposed method laser scanning point can retrieve missing data in clouds based on these frequency ranges. They reapplied the distance minimum spanning tree, obtained refined tree skeleton from tree-borne data, and used Laplace function to simplify tree skeletons. To rearrange 3D tree model, they estimated each branch's radius and then added leaves to create

crown shape. This advanced method was extensively evaluated using laser scan point maps of 10 different tree species on earth. The qualitative and quantitative indicators' evaluation shows that 3D method effectively formed tree model without an incomplete full laser scanning point cloud. The 3D morphable model is low-dimensional parameter of 3D objects and provides an effective way of bringing 3D geometry together with two dimensional (2D) images. However, because current transformation models are based on 3D scans, it is not feasible economically in budget category of general categories such as animals. Cashman *et al.* [18] have shown that models can be constructed from 2D images. They indicate that collecting 2D images of particular object category has enough information to create a 3D model with minimally distorted user manipulation, even without surface's texture. The main limitation is that the category needs to be emphasized in budget category, not providing an accurate model very close to average measure's first estimate. The model was represented by linear combination of subdivisions on the surface, and subdivision surfaces can be monitored. They presented results using various natural object classes and showed that very high-quality models could be obtained from this limited information. Laser scanning is a new technology that enables high-density, and accurate 3D measurements of objects. The development of scanners and laser technologies has led to many successful land and forest surveying, industrial design, and urban planning. However, pneumatic laser scanners are expensive and accurate enough not to penetrate farming or careful planning. On the other hand, tripod ground-based laser scanners are impractical to use. However, low-cost laser scanners could be installed in future. The purpose of the study by Lumme *et al.* [19] was to verify the use of scanners and laser spot data in agriculture and precision agriculture. They have developed an algorithm that can automatically determine and estimate ear size based on laser scanner data. This result is also related to grain yield, but finding suitable parameters for algorithms that give relative results rather than absolute grain yield is problematic. Glendell *et al.* [20] compared ground-based laser scanning with ground-based imaging structures of drones and moving terrain. They have used terrestrial laser scanning as benchmark and compare cost-effectiveness and accuracy of two types of structural exercise techniques for conducting investigations into highland landscape erosion. Besides, digital surface models derived from each technique were used to quantify expected soil loss in highland trenches. These estimates of gully overall erosion rate suggest that gully total erosion rates for floors and walls were three times higher than the previous estimates, the latter being primarily gullied walls characterize wind and raindrop erosion.

UAV photogrammetry technology has opened many new applications in different domains, providing an inexpensive alternative to traditional manned aerial photogrammetry technology for large-scale topographic maps and detailed 3D images. Jutzi *et al.* [21], proposed a new way to improve drone-based 3D mapping by combining laser and optical scanner data. They proposed installing two sensors on an unmanned aerial vehicle. First, used equipment is calibrated by camera's geometric calibration. Feature detection is then performed from series of images, considering the extracted points of interest and projected 3D laser points. These 2D results are fused with measured laser distance and added to beam for simultaneous positioning and 3D mapping. However, the derived photogrammetric product may be more accurate. In Nagai *et al.*'s research [22], an unmanned aerial vehicle (UAV) survey and mapping system was developed to obtain broader remote sensing coverage and advanced land survey details and accuracy at low cost. They have proposed a new method of direct georeferencing using bundle block-matching and Kalman filtering. This will automatically create detailed shapes and textures for drone-generated objects at low altitudes. Another study by Ilci *et al.* [23] aims to study drones' role in 3D mapping of archaeological locations. For this reason, two measurements were made at two different archaeological sites. Based on this study's results, field aeronautical charts and 3D models were created quickly and cost-effectively, and drone measurements were performed with cm to dm accuracy. Khanna *et al.* [24] described a framework for estimating crop height using data collected from an array of easily accessible monocular cameras and UAVs. This algorithm can automatically post-process point clouds created with crop height estimates using off-the-shelf photogrammetric software. The segmentation algorithm that separates plants from soil is essentially index-independent, but it is impossible to study multiple indexes' effectiveness for segmenting soil plants. There are different methods for segmenting and extracting the desired object from the image [25]. The results show that proposed method is superior to manual measurements.

Lan *et al.* [26] have used Clifford algebra's subalgebra, quaternion, as a local descriptor of color images. They suggested local descriptor called quaternion local ranking binary mode for color photos. Unlike traditional descriptors extracted individually from each color channel or vector representation, quaternion local ranking binary is well suited for quadrant representations of color images that use quaternions to encode color pixels. The binary mode quaternion process all color channels directly from quad domain and include their relationships simultaneously. The Clifford transform is applied to the quaternary ionic representation of color images. The local quadruple sort binary pattern uses a reference quadrupole to sort a quaternionic representation of two-color pixel and perform local binary coding in resulting phase to create color image for local descriptor. Experiments have shown that the binary position of local quadrant is better than some modern methods.

III. MATERIAL AND METHODS

i Remote sensing platform is extensively practiced in agriculture due to its numerous advantages, such as implementing new research techniques and data-rich assistance for crop identification and modeling. Remote sensing platform

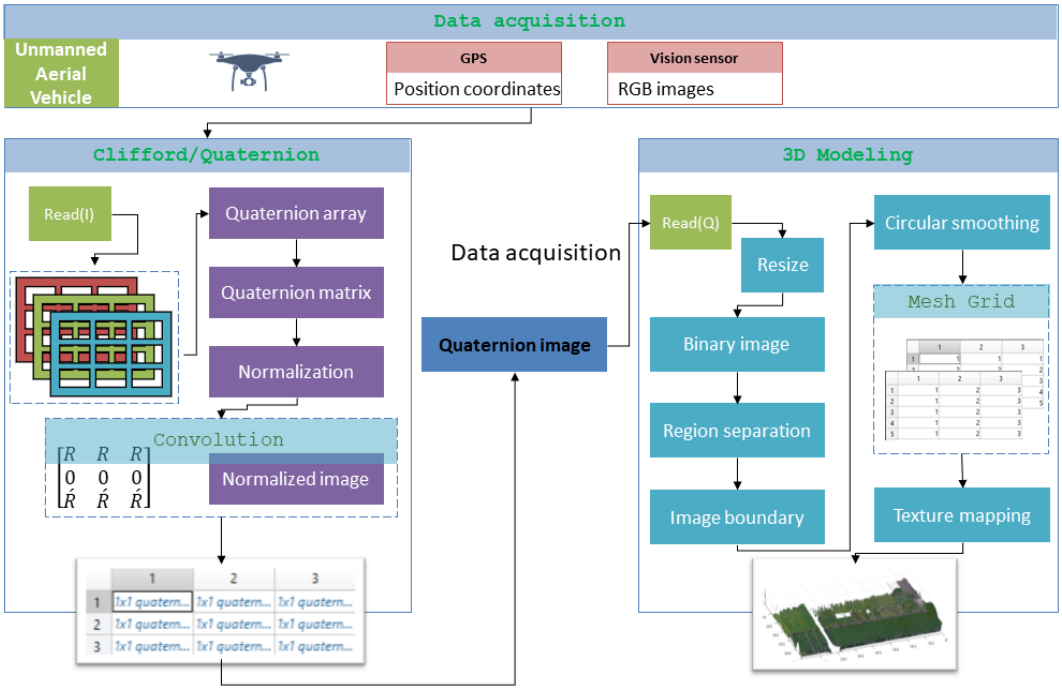

FIGURE 1. Structure of the proposed Clifford algebra-based 3D modeling.

also has benefits of wide coverage, compact revisits, comparatively inexpensive purchase costs, and novel role in surveying, evaluating, observing, and managing extensive farmland [27]. Stud based on unmanned aerial vehicles (UAV) have begun to gain momentum in recent years due to their advantages over traditional remote sensing platforms [28]. The proposed research consists of three stages. The first stage is to collect data using UAVs. The second stage is converting RGB image acquired from UAV into quaternion image, then the third stage is 3D modeling of that image. Figure 1 explicates the overall structure of suggested Clifford based 3D modeling.

A. DATA COLLECTION

RGB image data of agricultural land for simulation purposes is collected using quadrotor phantom. The image sensor was mounted on UAV to acquire the data.

1) STUDY SITE DESCRIPTION

Image data were collected at Faisalabad University Agricultural Farm in mild, sunny weather conditions. Faisalabad city is classified as a warm desert climate zone according to Köppen-Geiger classification system [29]. The research site was a 35m × 18m land with 17 different plants on different subplots. Each subplot's length was 18m × 1m, and distance between adjacent sites was one meter. Each lower panel consists of four rows of plants, with a row spacing of 0.3 m for each plant. Eight images were taken every two weeks. The above ground level (AGL) elevation was 50 meters, with two centimeters ground sampling distance. From January 1st to April 15th. We acquired images of size, i.e., 4000 × 3000 px. However, during simulation, size was reduced while preserving aspect ratio. Various images were taken at varying times, and Figure 2 is presented here for further testing and simulation purposes. The image file size is 5.25 MB, and the format is JPG. The research locality is an agricultural farm maintained by the University of Agriculture Faisalabad in Pakistan.

FIGURE 2. Original image acquired from UAV.

2) UNMANNED AERIAL VEHICLE

The quadrotor Phantom 4 is used as an unmanned aerial vehicle to acquire images from above ground level.

TABLE 1. Specifications of unmanned aerial vehicle.

Sr#	Attribute	Value
1	Total Weight	1280 g
2	Diagonal Size	350 mm
3	Ascent Speed (Max)	5 m/s
4	Descent Speed(Max)	3 m/s
5	Speed (Max)	16 m/s
6	Tilt Angle (Max)	35°
7	Angular Speed (Max)	150°/s
8	Flight Time (Max)	25 minutes
9	Operating Temperature Range	32° - 104°F
10	Satellite Positioning Systems	GPS/GLONASS

TABLE 2. Specifications of the image sensor.

Sr #	Attribute	Value
1	Sensor	1/2.3" CMOS
2	Lens	FOV 94° 20 mm
3	ISO Range	100-1600 (photo)
4	Shutter speed	8 - 1/8000 s
5	Size of test image	4000×3000
6	Max Video Bitrate	60 Mbps
7	Supported File Systems	FAT32 ; exFAT
8	Photo formate	JPEG, DNG (RAW)
9	Supported SD Cards	Micro SD
10	Operating Temperature Range	32°- 104°F

The Phantom 4 drone maintain and record all places of interest in flight. It also records complete flight route, flight time, flight area, and format assigned to images and record for future use [30]. Simultaneously, propelled flight recorder continually records information on all internal components of Phantom-4. Table 1 shows different attributes and their respective values for UAV. The flying was performed around mid-day to evade influence of shadows. Before the first flight, inertial measurement unit (IMU) and compass were calibrated only once as a set and did not require calibration later in operations. The Phantom 4 platform was integrated with custom payload consisting of multispectral camera, FirePoint TM100 GPS, and battery, as shown in Figure 3. The ADC microsensor is multispectral sensor with three fixed bands (red-green-NIR) compatible with LandState TM2, TM3, and TM4 functional bands. The GPS module and battery are directly connected to the basement of UAV. The ADC microsensor was housed in lightweight aluminum alloy frame with downward direction.

FIGURE 3. Payload attached with the Unmanned aerial vehicle.

3) SENSORS DESCRIPTION

We used Canon S95 with a 12-megapixel CCD sensor and an ISO range of 100-200 as UAV's RGB camera to acquire images. Inside the camera was Bayer RGB filter array with an Aptina CMOS sensor and a checkerboard pattern. The specifications of sensor are explained in Table 2. The ultra-lightweight sensor operates in wavelength range of 520 nm to 920 nm and is suitable for remote agricultural sensing applications.

B. QUATERNION FILTERING METHOD

The quaternion is the sub-algebra of Clifford algebra. A quaternion is a number in multi-dimensional space [31]. It has one real scalar part and three imaginary parts Vector,Bivector and Trivector as expressed in Equation 1. The quaternion Q can be expressed as Equation 2:

$$\left|\begin{array}{c} scalar = 1, \\ Vector = e_1, e_2, e_3, \\ Bivector = e_1e_2, e_2e_3, e_3, \\ Trivector = e_1e_1e_2e_3 \equiv I \end{array}\right| \tag{1}$$

$$Q = a_0 + a_1(Ie_1) - a_2(Ie_2) + a_3(Ie_3) \tag{2}$$

where Ie_1 is equal to $a_1e_2e_3$, Ie_2 is equal to $a_2e_3e_1$ and Ie_3 is equal to $a_3e_1e_2$. a represents real numbers that are used to represent complete multiple vectors. The quaternion representation of color images is generally used in the literature [32]. Let the three imaginary components of quaternion represent the three primary color components of red, green, and blue (RGB). The real part is 0, so quaternion function $q(x, y)$ can be expressed as Equation 3

$$q(x, y) = q_R(x, y) + q_G(x, y) + q_B(x, y) \tag{3}$$

where $q_R(x, y)$, $q_G(x, y)$,and $q_{B(x,y)}$ represents pixel values of red,green and blue respectively. The x and y here represent position of the specific pixel on x and y coordinates [33]. In geometric algebra, a rotor R, is an even-grade element of algebra which satisfies $R\hat{R} = 1$, where $\hat{R}$ stands for conjugate of R.

Using quaternion filtering method, colors can be represented and analyzed as a single entity. The colors can be processed as one unit instead of three separate channels: red, green, and blue [34]. The color texture model must consider each three-color channel's spatial interaction and interaction between the different color channels.

The process of converting RGB to quaternions begins with reading test image into an array. Algorithm 1 shows pseudo code for converting RGB to quaternion image. Since test image is color image, the array has three dimensions. A 3 × 3 mask is created and applied to test image that is converted to a quaternion. Quaternion mask consists of two

Algorithm 1 Pseudo Code for Converting RGB to Quaternion Image

```
im= read image(I)
mu = x + y + z/√3
R = S {cos π/4 + μ sin π/4}
left = [R R R; quaternion(zeros(1, 3)); conjugate([R R R])]
right = conjugate(left)
q_I = convolution(im)
Output = vector(q_I)
Display the result in an image window
```

parts, as explained in Equation 4. Where $R\hat{R}$ is a conjugate of R [35]. The left part contains R in the first row, $R\hat{R}$ in the last row, and right part is repositioned. The equation for R is explained in Equation 5 whereas conjugate of R is obtained using Equation 6 Where r represents total number of components and variable i is used to count these numbers in a loop.

$$\begin{vmatrix} R & R & R \\ 0 & 0 & 0 \\ \hat{R} & \hat{R} & \hat{R} \end{vmatrix} \times \begin{vmatrix} \hat{R} & \hat{R} & \hat{R} \\ 0 & 0 & 0 \\ R & R & R \end{vmatrix} \tag{4}$$

$$R = S\left\{\cos\tfrac{\pi}{4} + \mu \sin\tfrac{\pi}{4}\right\} \tag{5}$$

$$\hat{R} = \sum_{i=0}^{r} (-1)^{\frac{i(i+1)}{2}} R_i \tag{6}$$

$$\mu = \frac{x + y + z}{\sqrt{3}} \tag{7}$$

Referring to Equation 5, S denotes scale factor SF, and we use it to be $\sqrt{6}$. For a pixel distance value of one, scale factor will be $\sqrt{1}$, μ is a pure quaternion unit which is obtained by using Equation 7. This mask operator for quaternion $R\hat{R}$ discovered by Hamilton [36] defines how to rotate around axis. The conjugate of R reverses direction of rotation, i.e., $\hat{R}$. The upper row of the masked pair rotates pixel values by angle positive $\pi/2$, and lower row of the mask rotates pixel values by the angle negative $\pi/2$. After applying quaternion mask, we then save the output image. The last step of the first stage is converting the array to pure quaternion matrix and include RGB components in the w, x, y, and z components of quaternion matrix.

C. 3D MODELING

The 3D modeler of our proposed method first divides quaternion image into different areas based on dark edges. A 3D extension grid is created for each area. The original image texture is attached as stylized shadow to get 3D model of image. The proposed system later joins texture model with original image. The system supports affine transformations such as rotation, translation, and scaling. Algorithm 2 shows the pseudo-code for 3D modeling of image. It initializes by reading quaternion image and resizing that image. After that, different operations are applied to that image, such as converting into a binary image, filling holes, applying mask, region separation, and creating a mesh grid. These steps are explained further in the subsections.

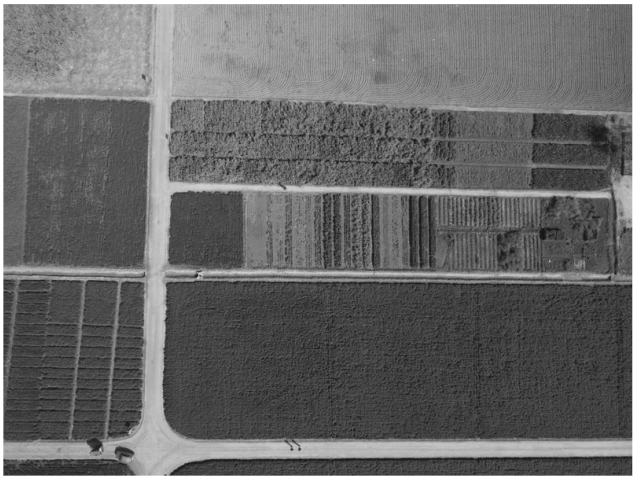

FIGURE 4. Output image of quaternion filtering method.

Algorithm 2 Pseudo Code for 3D Modeling of Image

```
im= read quaternion image(q)
resized_im = rows, (y×rows)/x
BW = imbinarize (resized_im)
rgn = label matrix(BW)
filled = imfill(BW,'holes')
mask = create boundary mask(BW)
B,L,N,A = bwboundaries(BW,'noholes')
for k 1:N do
    boundary = B_k
    if nnz(A(:,k)) > 0 then
        boundary = B_k
        for l find(A(:,k)) do
            boundary = B_l
        end for
    end if
end for
Calculate distance map
Apply Circular Smoothing
Create Mesh Grid
x = 1:size(H,1)
y = 1:size(H,2)
[X,Y] = meshgrid(y,x)
Texture Mapping
h = warp([X X],[Y Y],[H H])
show 3D figure
```

1) REGION SEPARATION

The quaternion filtering method's output image is passed to the 3D modeling part. The proposed process first extricates regions from image. Every region surrounded by dark edges forms an area and gives the initial segmented image. This method calculates curve points by applying non-maximum

suppression to second derivative of original image and then connects them to form structural curve. For some agricultural images, aforementioned process can immediately extract available contours. Though, if the input image contains noise, result will not be neat to process further.

2) FINDING IMAGE BOUNDARY

Using these segmented regions, the system expands them to remove edge pixels and then finds contour. Then extract region boundary from segmentation result. If there are holes or uneven borders, they will be repaired by system. Figure 5 shows the result of applying a boundary mask.

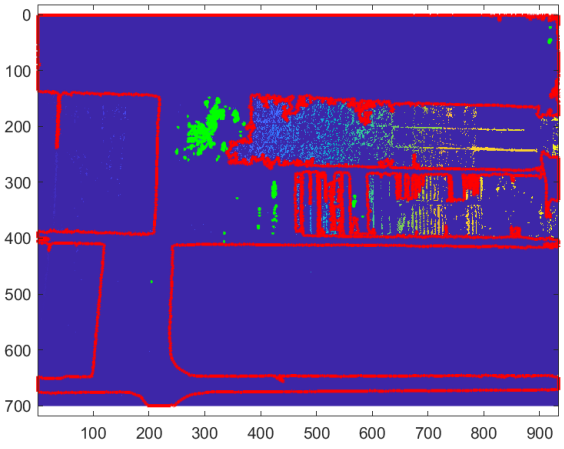

FIGURE 5. Result of applying boundary mask.

3) DISTANCE MAP AND MESH GRID

To detect the final contour from initial results, the system executes seed filling algorithm to find closed area. Then, it calculates Euclidean distance transform of binary image. Distance map and circular smoothing are performed using Algorithm 3. The distance transform will digitally assign distance between that pixel and nearest non-zero pixel for each pixel in image. The system applies fitting constraint Delaunay triangulation [37] to each boundary to obtain discrete domain. Figure 6 shows the distance map obtained from test image. Yellow color represents more height, and blue represents less height from the ground.

Using the inflation algorithm, function $f(x)$ corresponds to the region's expansion height. The resulting $f(x)$ produces a parabolic cross-section. Then, our system uses Equation 8 to transform it into smoother mesh. We have used these equations from the literature [38]. Where D_{max} represents maximum distance values of regions and a can be calculated using Equation 9. For areas that need to be kept flat, Neumann boundary conditions can be used.

$$H_{i,j} = \sqrt{D_{max}^2 - a^2} \tag{8}$$

$$a = D_{max} - D_{i,J} \tag{9}$$

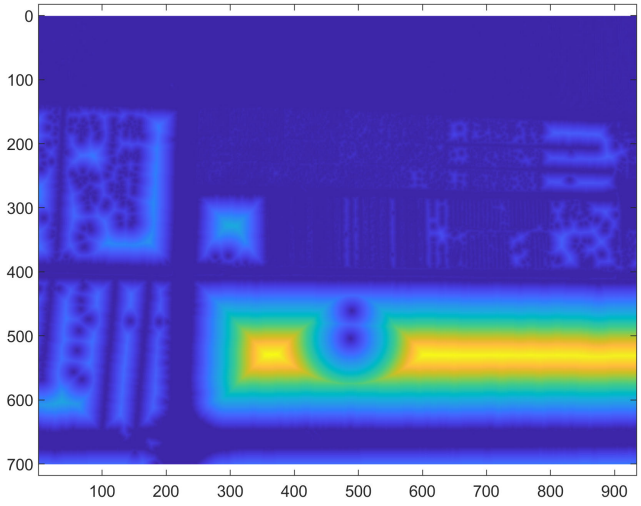

FIGURE 6. Distance map.

Algorithm 3 Algorithm for Distance Map and Circular Smoothing

```
Initialize D and rgn = label matrix
r = rgn_{1,1}
for i size_{D,1} do
    for j size_{D,2} do
        if rgn_{i,j} = r then
            D_{i,j} = NaN
        end if
    end for
end for
H= D
M = D_max
for i size_{D,1} do
    for j size_{D,2} do
        if rgn_{i,j} = r then
            a = m − D_{i,J}
            H_{i,j} = sqrt(m^2 − a^2)
        end if
    end for
end for
```

4) TEXTURE MAPPING

The original image is directly used to synthesize front texture. The proposed approach employs a heuristic rule when the area is far distant from the area border [39]. x, y coordinates are used as front's texture coordinates and directly attach to original image. The proposed approach initially chooses base color that contributes largest adjacent to edge in a given area. Our system then uses watershed algorithm to apply label-based segmentation to each area of original texture. The algorithm starts with binarization of input image. Later utilize distance transform to the binary image. Established this distance image as threshold furthermore do some morphological work to extricate regions from image. For each region, the contour is extracted to create seed of the watershed

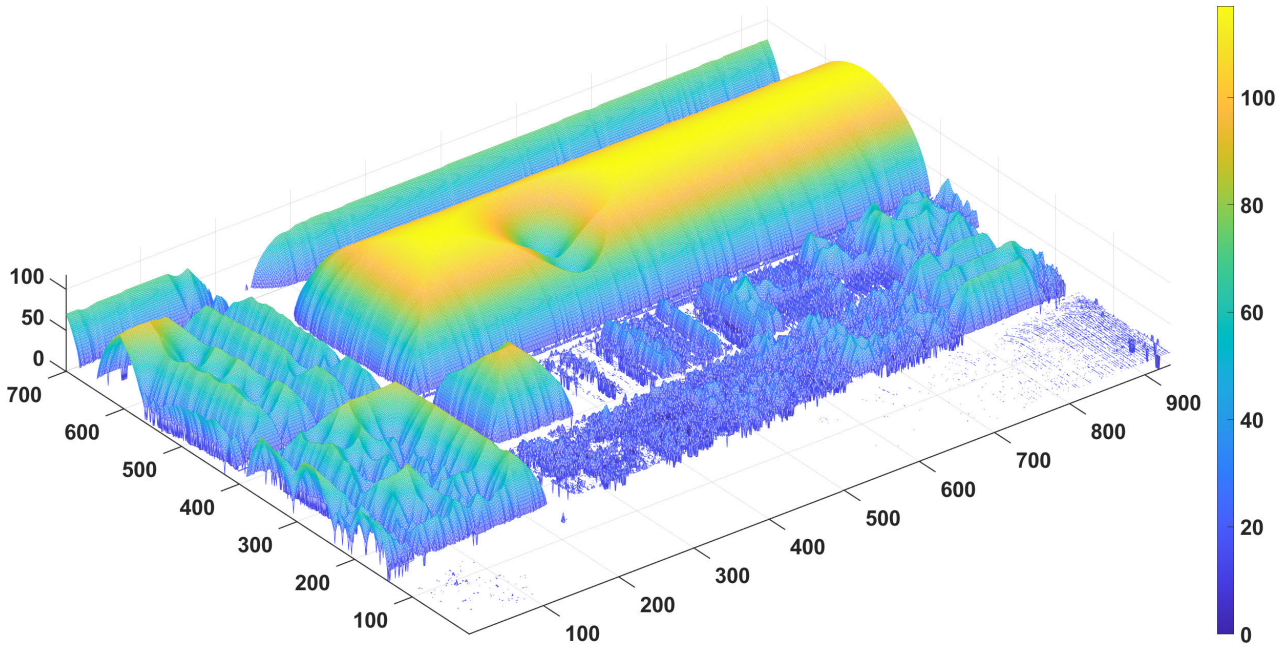

FIGURE 7. Mesh Plot.

algorithm. Later apply watershed algorithm and merge neighboring regions. To distinguish the distance from region's boundary, we apply distance transformation to the entire area and utilize this distance map to determine closest route from a specific region to the edge. By default, the produced meshes' centers are all positioned at the same depth at $z = 0$, and relativistic depth order may be undesirable. The transformation processes backed by system include transformation, scaling, and rotation.

5) RENDERING ON THE MESH

All meshes generated by our system are textured. Texture coordinates u, v are assigned to each vertex to render correctly on the mesh. For the previous, those coordinates are just x, y coordinates of the vertex. On the rear, v element of u, v is, however, the value of y, though u element is the aggregate of x plus 1. Therefore, texture coordinates greater than one indicate that the aforementioned vertex refers to a certain back surface. During rendering the mesh, system uses this information to determine which portion of the texture to examine.

IV. RESULTS AND COMPARISON

For simulation, we installed Matlab R2019b version 9.7. We tested our system on an Intel Core i7-1160G7 Processor at 4.40 GHz with a windows operation system.

To demonstrate our method's versatility, we select images acquired from the UAV of a composite of different crops. These images were captured during different stages of crop growth. Table 3 shows the test-bed implementation environment for simulations.

TABLE 3. Test-bed implementation environment.

System Component	Description
CPU	Intel Core (TM) i7-1160
RAM	16 GB
OS	Windows 10
Programming-Language	Matlab
Clifford Multivector Toolbox	Version 1.0
Image Processing Toolbox	Version 11.0
Quaternion Toolbox (QTFM)	Version 2.5
IDE (Platform)	Matlab R2019b (V 9.7)

The effectiveness of 3D images can be evaluated using two commonly used methods. The first method is structural similarity index measure (SSIM) [40] and the other is peak signal-to-noise ratio (PSNR) [41]. PSNR and SSIM indicators are often used to measure image quality. These pointers identify how good the change is after algorithm is applied to the image.

PSNR is an index of a statistical analysis based on the gray values of pixels in an image, an error that defines mean square error (MSE) between first image $I(i, j)$ and the redesigned output image $O(i, j)$. PSNR is defined using Equation 10 and MSE is calculated using Equation 11

$$PSNR = 10 \times \log_{10}\left(\frac{(2^n - 1)^2}{MSE}\right) \tag{10}$$

$$MSE = \frac{1}{mn}\sum_{i=0}^{m}\sum_{j=0}^{n}\|I(i, j) - O(i, j)\|^2 \tag{11}$$

where i, j shows the pixel position of input and output images on x and y coordinates. SSIM shows the similarity between two images. The first image is the original agricultural image

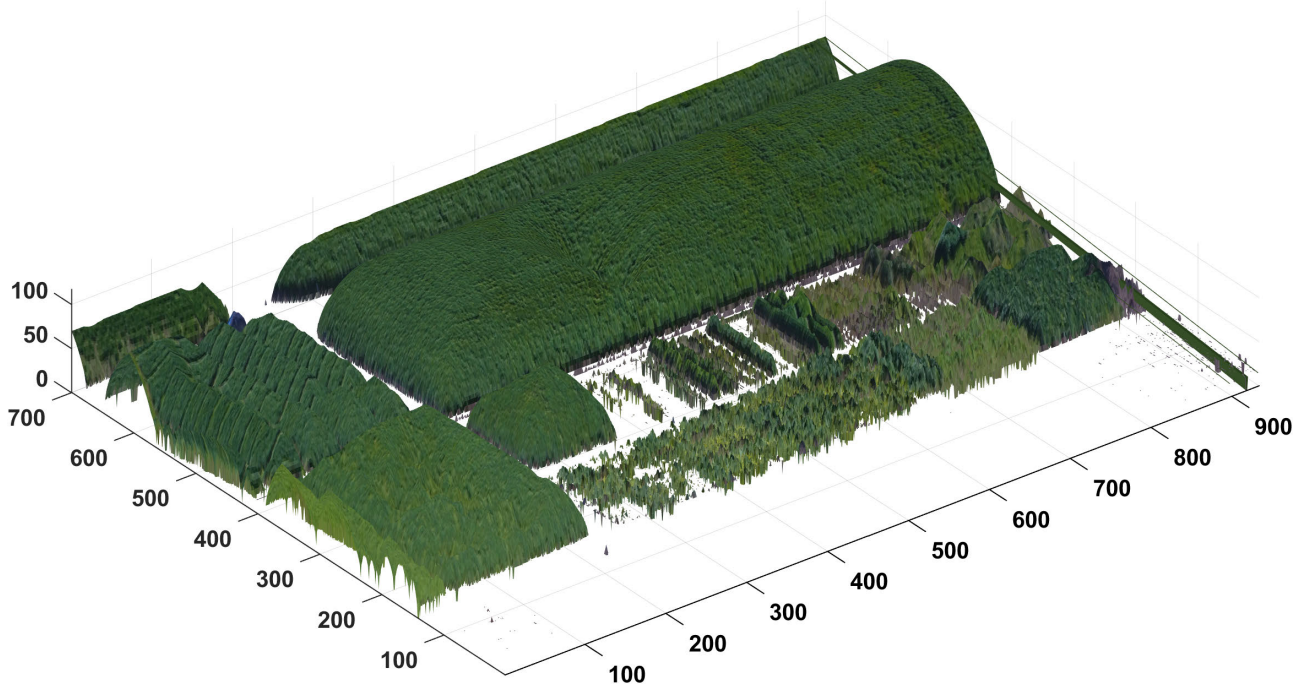

FIGURE 8. Three dimensional view of agricultural image.

acquired through UAV, and the other image is redesigned 3D image using Clifford geometric algebra-based approach. MSE for redesigned 3D image is calculated using the symmetric surface distance between the reconstructed image $O(i, j)$ and the original image $I(i, j)$ [42]. Symmetric surface distance is calculated using Equation 12. Where m and n represent the respective number of densely sampled points on input and output images. $d(p, O)$ represents the distance where p is the specific point belongs to input and output images.

$$d(I, O) = \frac{1}{m} \sum_{p \epsilon I} d(p, O) + \frac{1}{n} \sum_{\hat{p} \epsilon I} d(\hat{p}, I) \tag{12}$$

The similarities between $I(i, j)$ and $O(i, j)$ images and formats of these two images are explained as Equation 13

$$SSIM(I, O) = l(I, O)^{\alpha} \cdot c(I, O)^{\beta} \cdot s(I, O)^{\gamma} \tag{13}$$

where $l(I, O)$ represent the luminance, $c(I, O)$ represent the contrast, and $s(I, O)$ represent the structure of image. Here α, β, and γ are greater than 0. Equations for luminance, contrast, and structure are presented in 14, 15 and 16 respectively.

$$l(I, O) = \frac{2\mu_I \mu_O + C_1}{\mu_I^2 + \mu_O^2 + C_1} \tag{14}$$

$$c(I, O) = \frac{2\delta_I \delta_O + C_2}{\delta_I^2 + \delta_O^2 + C_2} \tag{15}$$

$$s(I, O) = \frac{\delta_{xy} + C_3}{\delta_I \delta_O + C_3} \tag{16}$$

where μ_I, and μ_O represent all pixels in image $I(i, j)$ and $O(i, j)$; δ_I and δ_O are the standard deviations of image pixel;

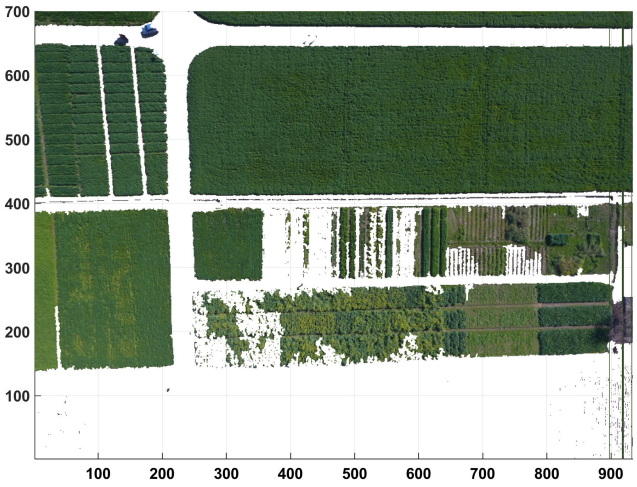

FIGURE 9. x-y View of three dimensional image.

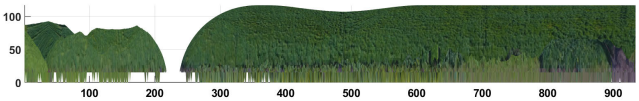

FIGURE 10. x-z View of three dimensional image.

and δ_{xy} is co-variance of image $I(i, j)$ and $O(i, j)$. C_1, C_2, and C_3 are constants that are employed to avoid the error when denominator of formula.

When the PSNR value is high, it shows the image restoration is good, and low PSNR shows bad results. The range

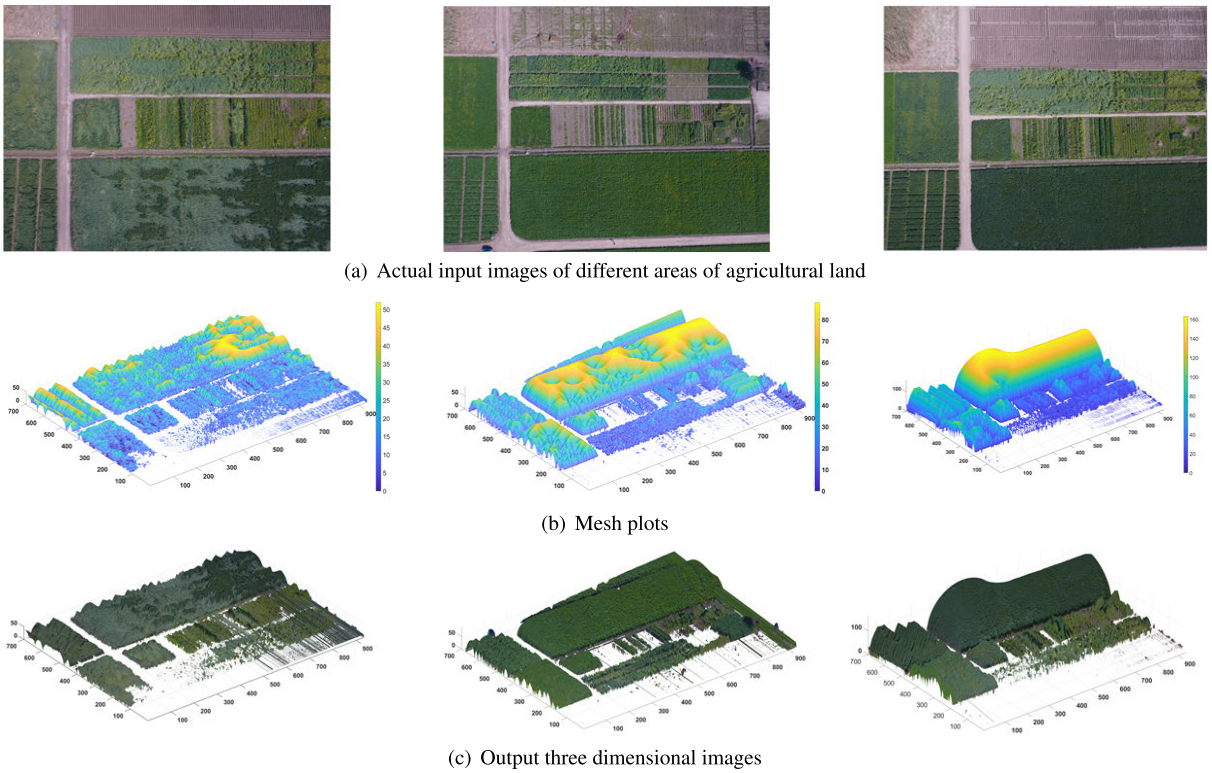

(a) Actual input images of different areas of agricultural land

(b) Mesh plots

(c) Output three dimensional images

FIGURE 11. Results of the proposed model on different images.

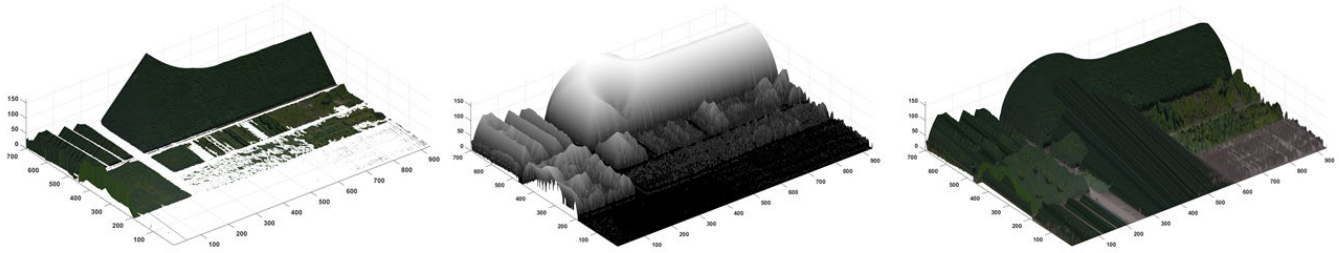

(a) (b) (c)

FIGURE 12. Visual output of (a) Ruma *et al.* [46], (b) Salih *et al.* [47], and (c) Koyuncu *et al.* [48].

structural similarity index measure is from 0 to 1. When SSIM value is equal to 1, it shows that structural similarity is good, and two images are same. [49]. From the comparison Table 4, it is clear that the proposed method performs well than the other approaches.

TABLE 4. PSNR and SSIM comparison of proposed model.

Sr # [Ref]	PSNR	SSIM
1 [43]	11.29	0.6307
2 [44]	13.21	0.4721
3 [45]	17.23	0.7542
4 [46]	13.61	0.5498
5 [47]	16.82	0.6834
6 [48]	15.56	0.6159
7 [Proposed]	17.73	0.8713

Clifford Algebra gives a more reliable framework to resolve the problem of image processing in frequency domain where the image frequency is not monochrome [50]. We utilize agricultural image shows in Figure 2 for the test purpose. By applying quaternion filter, we obtained the image 4. For fast processing, we resized this image and extracted regions from the image. The segmentation process is used to differentiate between crops and land regions. Region boundaries are then extracted from segmentation, as shown in Figure 5. We calculated distance map to insert each pixel's distance into nearest black pixel. The value of distance shows how many pixels the plane is spread out. We created a mesh map using distance map such as Figure 7. We merged the mesh plot with original image to obtain a three-dimensional view of agricultural land. Figure 8 shows the Three-dimensional

view of the agricultural image. X-Y view is shown in Figure 9 of three-dimensional output image, and Figure 10 shows the x-z view of output three-dimensional agricultural image.

Figure 11 shows Results of the proposed model on different images acquired at different stages of crop growth. Sub-Figure 11(a) shows the three input images acquired by UAV. Sub-Figure 11(b) shows the mesh plot of these images and Sub-Figure 11(c) shows the 3D output plot of these images respectively. From mesh plots, we can clearly observe the difference in the height of crops at different stages.

For the visual comparison, we have selected recently published work which are using different techniques. The last image of Figure 11 is used for the comparison with existing techniques. Figure 12 shows the Visual output of these techniques. Sub-Figure 12 (a) shows the output of Ruma *et al.*'s proposed algorithm. [46]. Which employs the depth hypothesis to obtain the 3D image after background and foreground segmentation. Sub-Figure 12 (b) shows the output of Salih *et al.*'s proposed 3D mesh reconstruction technique. [47]. Sub-Figure 12 (c) shows the output of Koyuncu *et al.*'s proposed method. [48].

V. CONCLUSION

3D modeling of crops performs a vital role in the field of remote sensing. The proposed method introduces quaternary algebra, a subfield of Clifford geometric algebra for 3D image reconstruction. Powerful geometric algebra provides mathematical tools for expressing and analyzing complex things in a multidimensional-unified framework. We have used an unmanned aerial vehicle to get images of crops. We applied various image processing techniques such as segmentation, distance map, mesh grid, and texturing on the quaternion image to obtain 3D image of agricultural land. This article contains a comparison table of peak signal-to-noise ratios and structural similarity indicators. A comparison table of peak signal-to-noise ratio and structural similarity index measure is included in this paper. We obtained a PSNR value of 17.73 and SSIM of 0.8713 using the Clifford algebra-based 3D modeling technique. The comparison outcomes explicate that the suggested approach has better PSNR and SSIM values. Future work will focus on designing different testing strategies and expanding the assessment scope to include various 3D reconstruction techniques.

REFERENCES

[1] B. A. Aubert, A. Schroeder, and J. Grimaudo, "IT as enabler of sustainable farming: An empirical analysis of farmers' adoption decision of precision agriculture technology," *Decis. Support Syst.*, vol. 54, no. 1, pp. 510–520, Dec. 2012.

[2] G. Hong and H. T. Abd El-Hamid, "Hyperspectral imaging using multivariate analysis for simulation and prediction of agricultural crops in Ningxia, China," *Comput. Electron. Agricult.*, vol. 172, May 2020, Art. no. 105355.

[3] P. S. Thenkabail, J. W. Knox, M. Ozdogan, M. K. Gumma, R. G. Congalton, Z. T. Wu, C. Milesi, A. Finkral, M. Marshall, I. Mariotto, and S. You, "Assessing future risks to agricultural productivity, water resources and food security: how can remote sensing help?" *PE RS, Photogramm. Eng. Remote Sens.*, vol. 78, no. 8, pp. 773–782, 2012.

[4] C. C. de Araujo Barbosa, P. M. Atkinson, and J. A. Dearing, "Remote sensing of ecosystem services: A systematic review," *Ecol. Indicators*, vol. 52, pp. 430–443, May 2015.

[5] J. Wilson, C. Zhang, and J. Kovacs, "Separating crop species in northeastern Ontario using hyperspectral data," *Remote Sens.*, vol. 6, no. 2, pp. 925–945, Jan. 2014.

[6] F. Librán-Embid, F. Klaus, T. Tscharntke, and I. Grass, "Unmanned aerial vehicles for biodiversity-friendly agricultural landscapes—A systematic review," *Sci. Total Environ.*, vol. 732, Aug. 2020, Art. no. 139204.

[7] W. E. Baylis, *Clifford (Geometric) Algebras: With Applications to Physics, Mathematics, and Engineering*. Berlin, Germany: Springer, 2012.

[8] S. Franchini, A. Gentile, F. Sorbello, G. Vassallo, and S. Vitabile, "ConformalALU: A conformal geometric algebra coprocessor for medical image processing," *IEEE Trans. Comput.*, vol. 64, no. 4, pp. 955–970, Apr. 2015.

[9] K. Sau, R. K. Basak, and A. Chanda, "Color image compression based on block truncation coding using clifford algebra," in *Information Systems Design and Intelligent Applications*. New Delhi, India: Springer, 2015, pp. 675–684.

[10] J. Vaz, Jr., and S. Mann, "On the clifford algebraic description of the geometry of a 3D Euclidean space," 2019, *arXiv:1908.08110*. [Online]. Available: http://arxiv.org/abs/1908.08110

[11] N. Liu, B. Lin, L. Yuan, G. Lv, Z. Yu, and L. Zhou, "An interactive indoor 3D reconstruction method based on conformal geometry algebra," *Adv. Appl. Clifford Algebras*, vol. 28, no. 4, p. 73, Sep. 2018.

[12] Z. Yu, J. Wang, W. Luo, Y. Hu, L. Yuan, and G. Lü, "A dynamic evacuation simulation framework based on geometric algebra," *Comput., Environ. Urban Syst.*, vol. 59, pp. 208–219, Sep. 2016.

[13] J. P. Yuan, Z. Fang, Y. C. Wang, S. M. Lo, and P. Wang, "Integrated network approach of evacuation simulation for large complex buildings," *Fire Saf. J.*, vol. 44, no. 2, pp. 266–275, Feb. 2009.

[14] A. B. Cahyono and R. A. Zayd, "Rapid mapping of landslide disaster using UAV-photogrammetry," *J. Phys., Conf. Ser.*, vol. 974, Mar. 2018, Art. no. 012046.

[15] C. Potena, R. Khanna, J. Nieto, R. Siegwart, D. Nardi, and A. Pretto, "AgriColMap: Aerial-ground collaborative 3D mapping for precision farming," *IEEE Robot. Autom. Lett.*, vol. 4, no. 2, pp. 1085–1092, Apr. 2019.

[16] A. Piron, F. van der Heijden, and M. F. Destain, "Weed detection in 3D images," *Precis. Agricult.*, vol. 12, no. 5, pp. 607–622, Oct. 2011.

[17] Z. Wang, L. Zhang, T. Fang, P. T. Mathiopoulos, H. Qu, D. Chen, and Y. Wang, "A structure-aware global optimization method for reconstructing 3-D tree models from terrestrial laser scanning data," *IEEE Trans. Geosci. Remote Sens.*, vol. 52, no. 9, pp. 5653–5669, Sep. 2014.

[18] T. J. Cashman and A. W. Fitzgibbon, "What shape are dolphins? Building 3D morphable models from 2D images," *IEEE Trans. Pattern Anal. Mach. Intell.*, vol. 35, no. 1, pp. 232–244, Jan. 2013.

[19] J. Lumme, M. Karjalainen, H. Kaartinen, A. Kukko, J. Hyyppä, H. Hyyppä, A. Jaakkola, and J. Kleemola, "Terrestrial laser scanning of agricultural crops," *Int. Arch. Photogramm. Remote Sens. Spat. Inf. Sci*, vol. 37, pp. 563–566, Jul. 2008.

[20] M. Glendell, G. McShane, L. Farrow, M. R. James, J. Quinton, K. Anderson, M. Evans, P. Benaud, B. Rawlins, D. Morgan, L. Jones, M. Kirkham, L. DeBell, T. A. Quine, M. Lark, J. Rickson, and R. E. Brazier, "Testing the utility of structure-from-motion photogrammetry reconstructions using small unmanned aerial vehicles and ground photography to estimate the extent of upland soil erosion," *Earth Surf. Processes Landforms*, vol. 42, no. 12, pp. 1860–1871, Sep. 2017.

[21] B. Jutzi, M. Weinmann, and J. Meidow, "Improved UAV-borne 3d mapping by fusing optical and laserscanner data," *ISPRS-Int. Arch. Photogramm., Remote Sens. Spatial Inf. Sci.*, vols. XL-1/W2, pp. 223–228, Aug. 2013.

[22] M. Nagai, T. Chen, R. Shibasaki, H. Kumagai, and A. Ahmed, "UAV-borne 3-D mapping system by multisensor integration," *IEEE Trans. Geosci. Remote Sens.*, vol. 47, no. 3, pp. 701–708, Mar. 2009.

[23] V. Ilci, I. M. Ozulu, S. Bilgi, and R. M. Alkan, "The usage of unmanned aerial vehicles (UAVs) for 3D mapping of archaeological sites," in *Proc. Feb-Fresenius Environ. Bull.*, 2019, p. 968.

[24] R. Khanna, M. Moller, J. Pfeifer, F. Liebisch, A. Walter, and R. Siegwart, "Beyond point clouds–3D mapping and field parameter measurements using UAVs," in *Proc. IEEE 20th Conf. Emerg. Technol. Factory Autom. (ETFA)*, Sep. 2015, pp. 1–4.

[25] D. Hazra and Y.-C. Byun, "OEBR-GAN: Object extraction and background recovery generative adversarial networks," *IEEE Access*, vol. 8, pp. 135730–135741, 2020.

[26] R. Lan, Y. Zhou, and Y. Y. Tang, "Quaternionic local ranking binary pattern: A local descriptor of color images," *IEEE Trans. Image Process.*, vol. 25, no. 2, pp. 566–579, Feb. 2016.

[27] D. Feng, W. Xu, Z. He, W. Zhao, and M. Yang, "Advances in plant nutrition diagnosis based on remote sensing and computer application," *Neural Comput. Appl.*, vol. 32, pp. 16833–16842, Jan. 2019.
[28] A. Bhardwaj, L. Sam, Akanksha, F. J. Martín-Torres, and R. Kumar, "UAVs as remote sensing platform in glaciology: Present applications and future prospects," *Remote Sens. Environ.*, vol. 175, pp. 196–204, Mar. 2016.
[29] M. C. Peel, B. L. Finlayson, and T. A. McMahon, "Updated world map of the Köppen-Geiger climate classification," Eur. Geosci. Union, Munich, Germany, Tech. Rep. hal-00305098, 2007.
[30] Y. Taddia, F. Stecchi, and A. Pellegrinelli, "Using DJI phantom 4 RTK drone for topographic mapping of coastal areas," *ISPRS-Int. Arch. Photogramm., Remote Sens. Spatial Inf. Sci.*, vols. XLII–2/W13, pp. 625–630, Jun. 2019.
[31] B. Chen, C. Zhou, B. Jeon, Y. Zheng, and J. Wang, "Quaternion discrete fractional random transform for color image adaptive watermarking," *Multimedia Tools Appl.*, vol. 77, no. 16, pp. 20809–20837, Aug. 2018.
[32] B. Chen, H. Shu, G. Coatrieux, G. Chen, X. Sun, and J. L. Coatrieux, "Color image analysis by quaternion-type moments," *J. Math. Imag. Vis.*, vol. 51, no. 1, pp. 124–144, Jan. 2015.
[33] U. A. Bhatti, Z. Yu, J. Li, S. A. Nawaz, A. Mehmood, K. Zhang, and L. Yuan, "Hybrid watermarking algorithm using clifford algebra with Arnold scrambling and chaotic encryption," *IEEE Access*, vol. 8, pp. 76386–76398, 2020.
[34] L. Shi and B. Funt, "Quaternion color texture segmentation," *Comput. Vis. Image Understand.*, vol. 107, nos. 1–2, pp. 88–96, Jul. 2007.
[35] P. W. Khan, G. Xu, M. A. Latif, K. Abbas, and A. Yasin, "UAV's agricultural image segmentation predicated by clifford geometric algebra," *IEEE Access*, vol. 7, pp. 38442–38450, 2019.
[36] W. R. Hamilton, *Elements of Quaternions*. White Plains, NY, USA: Longman, 1866.
[37] J. R. Shewchuk, "Delaunay refinement algorithms for triangular mesh generation," *Comput. Geometry*, vol. 22, nos. 1–3, pp. 21–74, May 2002.
[38] L. Feng, X. Yang, and S. Xiao, "Magictoon: A 2D-to-3D creative cartoon modeling system with mobile AR," in *Proc. IEEE Virtual Reality (VR)*, Jun. 2017, pp. 195–204.
[39] L. Feng, X. Yang, S. Xiao, and F. Jiang, "An interactive 2D-to-3D cartoon modeling system," in *Proc. Int. Conf. Technol. E-Learn. Digit. Entertainment*. Cham, Switzerland: Springer, 2016, pp. 193–204.
[40] U. Sara, M. Akter, and M. S. Uddin, "Image quality assessment through FSIM, SSIM, MSE and PSNR—A comparative study," *J. Comput. Commun.*, vol. 07, no. 03, pp. 8–18, 2019.
[41] Z. Wang, A. C. Bovik, H. R. Sheikh, and E. P. Simoncelli, "Image quality assessment: From error visibility to structural similarity," *IEEE Trans. Image Process.*, vol. 13, no. 4, pp. 600–612, Apr. 2004.
[42] X. Han, H. Laga, and M. Bennamoun, "Image-based 3D object reconstruction: State-of-the-art and trends in the deep learning era," *IEEE Trans. Pattern Anal. Mach. Intell.*, early access, Nov. 21, 2019, doi: 10.1109/TPAMI.2019.2954885.
[43] A. Ahar, D. Blinder, T. Bruylants, C. Schretter, A. Munteanu, and P. Schelkens, "Subjective quality assessment of numerically reconstructed compressed holograms," in *Proc. 38th Appl. Digit. Image Process.*, vol. 9599, 2015, p. 95990K.
[44] J. Torres-Sánchez, A. I. de Castro, J. M. Peña, F. M. Jiménez-Brenes, O. Arquero, M. Lovera, and F. López-Granados, "Mapping the 3D structure of almond trees using UAV acquired photogrammetric point clouds and object-based image analysis," *Biosyst. Eng.*, vol. 176, pp. 172–184, Dec. 2018.
[45] Z. Hu, J. Tang, P. Zhang, and B. P. Patlolla, "Identification of bruised apples using a 3-D multi-order local binary patterns based feature extraction algorithm," *IEEE Access*, vol. 6, pp. 34846–34862, 2018.
[46] S. Ruma, "2D–3D image conversion," *Int. J. Res. Eng., Sci. Manage.*, vol. 3, no. 1, pp. 389–392, 2020.
[47] O. M. Salih, M. H. Rasheed, M. M. Siddeq, and M. A. Rodrigues, "Image compression for quality 3D reconstruction," *J. King Saud Univ.-Comput. Inf. Sci.*, Jul. 2020.
[48] B. Koyuncu and R. Hameed, "Converting 2D pictures in JPEG into 3D objects in space," *Int. J. Eng. Sci.*, vol. 9, no. 1, pp. 15–20, 2020.
[49] J. Zhang, L.-R. Gong, K. Yu, X. Qi, Z. Wen, Q. Hua, and S. H. Myint, "3D reconstruction for super-resolution CT images in the Internet of health things using deep learning," *IEEE Access*, vol. 8, pp. 121513–121525, 2020.
[50] L. Dorst, C. Doran, and J. Lasenby, *Applications of Geometric Algebra in Computer Science and Engineering*. Berlin, Germany: Springer, 2012.

PRINCE WAQAS KHAN received the master's degree in computer science from the University of Agriculture Faisalabad, Pakistan, in 2017. He is currently pursuing the Ph.D. degree with the Machine Learning Laboratory, Department of Computer Engineering, Jeju National University, Jeju, South Korea. He has served as a Lecturer for the Department of Computer Science, University of Agriculture Faisalabad. He also worked as a Researcher with the Chongqing Key Laboratory of Cyberspace and Information Security, Chongqing University of Posts and Telecommunications, Chongqing, China. His research interests include artificial intelligence, machine learning, image processing, blockchain, and the Internet of Things.

YUNG-CHEOL BYUN studied at the University of Florida as a Visiting Professor from 2012 to 2014. He directs the Machine Learning Laboratory, Department of Computer Science. Before joining Jeju National University, he worked as a Special Lecturer with Samsung Electronics Company Ltd., in 2000 and 2001. From 2001 to 2003, he was a Senior Researcher with the Electronics and Telecommunications Research Institute (ETRI). He was promoted to join Jeju National University as an Assistant Professor in 2003. He is currently serving as a Director for the Information Science Technology Laboratory and other academic societies. He has been hosting an international conference, Computer, Network, Systems, and Industrial Engineering (CNSI), and serving as a program chair, a workshop chair, and a session chair for various international conferences and workshops.

MUHAMMAD AHSAN LATIF received the Ph.D. degree in computer science from Alpen-Adria University, Klagenfurt, Austria, in 2011. He is currently serving as an Assistant Professor for the Department of Computer Science, University of Agriculture Faisalabad, Pakistan. His research interests include modeling, image processing, computer vision, and artificial intelligence in agricultural context. Among his contributions are research articles, book chapters, and research projects. He leads a research group on using unmanned aerial systems and vision sensors to map crop phenology.